Atmospheric-pressure silica-like thin film deposition using 200 kHz/13.56 MHz dual frequency excitation

Y. Liu,[1,2] F. M. Elam,[3] E. Zoethout,[1] S. A. Starostin,[4] M. C. M. van de Sanden,[1,2] and H. W. de Vries[1,5]

[1]*Dutch Institute for Fundamental Energy Research, Eindhoven, 5612 AJ, The Netherlands*
[2]*Eindhoven University of Technology, Eindhoven, 5612 AZ, The Netherlands*
[3]*Advanced Research Centre for Nanolithography, Amsterdam, 1098 XG, The Netherlands*
[4]*FUJIFILM Manufacturing Europe B.V., Tilburg, 5047 TK, The Netherlands*
[5]*FONTYS Hogescholen, Eindhoven, 5612 MA, The Netherlands*

Email: H.W.deVries@differ.nl

Abstract: Atmospheric pressure plasma enhanced chemical vapour deposition (AP-PECVD) was used to synthesize silica-like thin films on polyethylene 2, 6 naphthalate (PEN) substrate with hexamethyldisiloxane (HMDSO) as the precursor and $Ar/O_2/N_2$ mixture as the working gas. A dual frequency (DF) excitation consisting of 200 kHz and 13.56 MHz frequencies was employed as the plasma source. The results have shown that compared to the single LF discharges, the DF excitation helps to improve plasma uniformity with less filaments. This could help to reduce the macro-defects and therefore to improve the permeation performance of the barriers. Besides, due to the increased electron density and gas temperature, the DF excitation demonstrates a more efficient breaking of $Si\text{-}CH_3$ bonds and therefore more oxidized structures of the deposited silica-like thin films.

1. Introduction

Encapsulation foils are essential to the flexible electronics industry e.g. electronic paper, flexible solar cells, quantum dot liquid crystal displays (QDLCDs), organic light-emitting diodes (OLEDs) and so on [1–5]. These encapsulation foils are designed primarily to protect electronic devices against degradation from oxygen and water [1–6], thus prolonging device lifetimes and improving operational stability. The foils should have excellent functional properties e.g. a low permeability of water and oxygen. Besides, they should also fulfil a specific set of requirements in terms of optical, smoothness, thermal, chemical, mechanical, electrical and magnetic properties [7]. In addition, commercialization of the flexible encapsulation foils further requires easier and continuous processing, a larger scale production, a higher throughput and a lower cost. Atmospheric pressure plasma enhanced chemical vapour deposition (AP-PECVD) is a novel technology to potentially achieve the industrial targets for commercial manufacturing of the flexible encapsulation foils. It could enable a precise control of the barrier layer properties e.g. thickness, density, porosity and morphology that determine the final encapsulating performance of the foils [8]. Meanwhile, due to its capability of in-line processing in an open reactor under atmospheric pressure, expensive large-footprint vacuum equipment can be avoided, and thus a considerable cost efficiency can be achieved in comparison to the common low-pressure plasma methods [9].

Previously, a scalable roll-to-roll AP-PECVD system operating at ~200 kHz frequency was developed to produce ultra-smooth 100 nm silica-like thin films on a polyethylene 2, 6 naphthalate (PEN) substrate in atmospheric pressure air [10]. The deposited thin films demonstrated an effective water vapor transmission rate (WVTR) of 1.8×10^{-3} g m^{-2} d^{-1} (at 40 °C, 90% relative humidity (RH)) [11]. Furthermore, by using a bilayer architecture, excellent encapsulation performances as low as 2×10^{-4} g

Public

m^{-2} d^{-1} was achieved [12]. AP-PECVD has therefore shown particular promise as a technique in the field of protective layers for photovoltaics and thin film transistors [6,13]. However, this technique is also intended to protect flexible OLEDs, which have a significantly more demanding WVTR requirement of 1×10^{-6} g m^{-2} d^{-1} (at 25 °C, 40% RH) [14,15]. Thus more works are required to further improve the permeation performance of the deposited silica-like thin films. It was found that a higher power density allows the synthesis of silica-like films with an improved microstructure and a lower impurity level resulting in excellent gas diffusion barrier properties [16,17]. Furthermore, an increased plasma power density is also required to enhance the deposition rate and thus the throughput of the thin films. However, when the input plasma power increases, there is a higher possibility that the uniform discharge will transits into a filamentary discharge [9,18]. The filamentary discharge is not suitable for the high-quality thin film deposition as the plasma filamentation is likely to result in the formation of macro-defects such as pinholes in the deposited thin films that limit the barrier permeation performance [12]. If the input power is further increased, the filamentary discharge can further transits into a high-current arc. The occurrence of an arc is usually accompanied by a high current density, an ultra-bright light emission and a local high temperature, which in turn may lead to electrical circuit damage, polymeric substrate burning, surface pollution or even damage to the electrode. Therefore, a novel technology to increase the plasma power while maintaining a homogeneous mode therefore is highly required to further improve the barrier properties and the throughput of AP-PECVD.

Recently, we reported on atmospheric-pressure diffuse dielectric barrier discharges (DBDs) using a dual frequency (DF) excitation at 200 kHz low frequency (LF) and 13.56 MHz radio frequency (RF) [19–21]. The DF excitation was previously discussed by many groups mainly in low-pressure plasmas [22–25]. It was found that in low-pressure DF plasmas, the phase relations between the two frequencies and stochastic (or collisionless) heating play an important role in the plasma mechanism [26–30]. The DF excitation can facilitate separate control of the plasma densities and energies [23,24,26,31,32] to induce modification of plasma reactivity, chemistry and thin film properties [33–38]. Under atmospheric pressure, however, due to the high gas density and the more frequent collisions between ions with electrons the gas molecules, the ion energy becomes very small [39]. The focus of DF excitation is on controlling the plasma parameters e.g. gas temperature, electron density and ion flux to the substrate [19,40]. According to the previous work from our group, the atmospheric-pressure DF excitation results in a time-varying electric field which is determined by the total LF and RF gas voltage and the spatial ion distribution which only responds to the LF component. By tuning the amplitude ratio of the superimposed LF and RF signals, the DF discharge reveals capability of temporally modulating the electric field and therefore the excitation/ionization mechanism, which can be a potential approach to modify the properties e.g. the chemical microstructure of the deposited thin films [19]. Moreover, due to the periodic oscillation of the RF electric field, the electron acceleration and thus the gas ionization is temporally modulated during each RF cycle. The RF electric field facilitates improved stability and uniformity of AP-DBDs simultaneously allowing a higher input power. This makes the DF excitation a potential approach to achieve a higher efficiency of the AP-PECVD process [20,21].

In this study, the 200 kHz/13.56 MHz DF excitation was employed as the plasma source for AP-PECVD. The gas mixture used in this study contained Ar, O_2, N_2 and hexamethyldisiloxane (HMDSO) as the precursor (similar to the conditions in the previous work [41,42]). The aim of the present work is to understand the plasma behaviour, the precursor dissociation and the deposition mechanism using the DF excitation. The paper is structured as follows: The experimental set-up for AP-PECVD and the analysing methods of the silica-like thin films are introduced in Section 2. The results including the electrical characteristics, the plasma emissions and the deposited silica-like barrier characteristics i.e. microstructure and surface morphology are presented in Section 3. Finally, the conclusions are drawn in Section 4.

2. Experimental setup

A schematic of the roll-to-roll AP-PECVD reactor is presented in Figure. 1. The discharge was ignited between a flat bottom electrode and a curved top electrode with a radius of 60 mm and a width of 45 mm. Both electrodes were covered by 0.1 mm thick polyethylene 2, 6 naphthalate (PEN) foil (Teonex Q65HA, Teijin DuPont Films) as the dielectrics. The electrode temperature was maintained at 30 ℃ by

Public

means of an oil circulation system. The smallest distance between the two electrodes was 1.0 mm. The gas mixture was injected from the left side of the discharge area in Figure. 1, while the substrates were transported at 40 mm/min in the same direction as the gas flow. The flow rate of the gas mixture ($Ar/O_2/N_2$) was controlled at 5 slm/0.2 slm/1 slm (standard litre per minute). The precursor, hexamethyldisiloxane ($C_6H_{18}OSi_2$, HMDSO), was injected via a controlled gas bubbler with a fixed argon flow rate of 0.3 slm. The amount of the precursor was calibrated as about 5 g/h. The DBD was excited by 200 kHz LF (SEREN L3001) and 13.56 MHz RF (SEREN R601) power sources which were superimposed and applied to the top electrode through a home-made matching circuit. The injected power of both the power sources was modulated at 625 Hz with a pulse width of 800 μs and a duty cycle of 50%. The discharge was first ignited by applying the LF power, and the RF power was applied after the discharge was stable. In this study, in order to investigate the influence of power composition on the plasma behaviour and thus the thin film deposition, both LF and DF discharges with an increasing power were obtained. The input power density was about 15-30 W/cm^2. The deposition time was about 23 s.

The discharge voltage and current were measured by a high voltage probe (Tektronix P6015A) with 75 MHz bandwidth and a current transformer (Pearson model 4100), respectively. An intensified charge-coupled device (ICCD) camera (PI MAX3), triggered by the applied voltage, was employed to collect the discharge emission from the side view of the gas gap with a macro lens (Tamron AF 90 mm). Attenuated total reflectance-Fourier transform infrared (ATR-FTIR) absorption spectroscopy was performed using *un*-polarized light (Frontier FT-IR/FIR Spectrometer, Perki- nElmer; Frontier UATR Ge/Ge, PerkinElmer) with one internal reflection to investigate the silica-like network structure of the barrier layers, with particular focus upon the Si-O-Si, Si-CH_3, and Si-OH spectral peaks. The surface morphology was characterized by dual-beam focused ion beam scanning electron microscopy (FIB-SEM) (Nova 600i Nanolab, FEI Company).

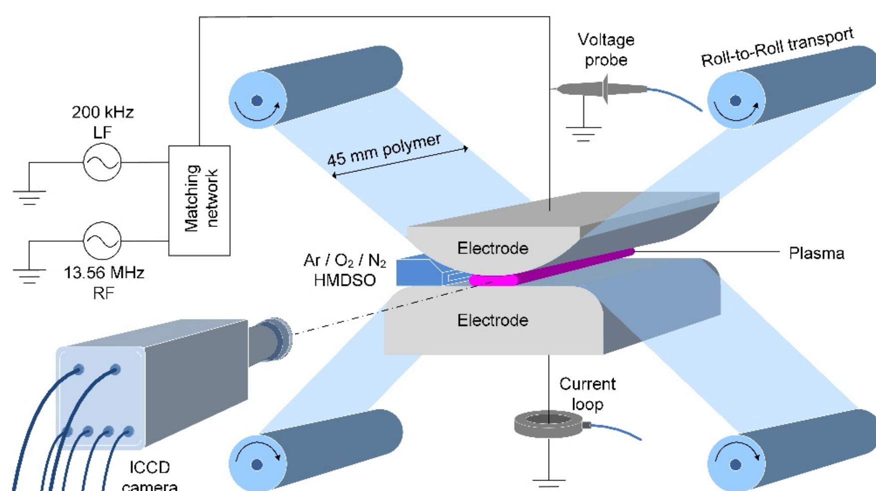

Figure. 1. Experimental set-up for atmospheric pressure plasma enhanced chemical vapour deposition (AP-PECVD) using 200 kHz/13.56 MHz dual-frequency (DF) excitation.

3. Results and discussions

The main purpose of this work is to investigate the influence of the DF excitation on the plasma behaviour and the resulting thin film properties. Therefore, the experimental conditions e.g. the gas mixture ($Ar/O_2/N_2$ flow rate and HMDSO concentration) were kept the same. Only the input power was changed e.g. with LF or DF power, total input power increasing from 100 W to 200 W. The plasma behaviour i.e. the electrical characteristics and the discharge emission together with the deposited thin film properties i.e. the microstructure and the surface morphology are discussed as follows.

Public

3.1 Electrical characteristics

Representative voltage-current waveforms of a single LF discharge (P_{LF} = 200 W) and a DF discharge (P_{LF} = 100 W, P_{RF} = 100 W) are shown in Figure. 2(a) and (b), respectively. For the LF discharge, the current exhibits typical electrical behaviour of a multi-pulse discharge [43] comprising three separate current peaks during each half cycle, see Figure. 2(a). Note that the current contains both discharge and displacement components. For the DF discharge, both the voltage and the current contain 200 kHz LF and 13.56 MHz RF frequencies. The LF component of the current also includes multi peaks, however the amplitude is much lower, see Figure. 2(b).

By doing fast Fourier transform (FFT) of the original waveforms, the LF and RF components are separated. The FFT amplitudes of the voltage and current as a function of the input power are presented in Figure. 3. For the single LF discharge, with the input LF power increasing from 100 W to 200 W, the LF voltage increases from 2.16 kV to 2.57 kV, and the LF current increases from 0.07 A to 0.12 A, see Figure. 3(a). For the DF discharge, the LF power is maintained at 100 W, and the RF power is increased from 0 W to 100 W. As a result, the RF voltage gradually increases from 0 kV to 0.62 kV. The LF voltage however slightly reduces from 2.16 kV to 1.99 kV, which is attributed to the not well performed matching network in this study. Moreover, the LF current gradually increases from 0.07 A to 0.08 A, and the RF current is significantly enhanced from 0 A to 0.26 A mainly due to the displacement component, see Figure. 3(b).

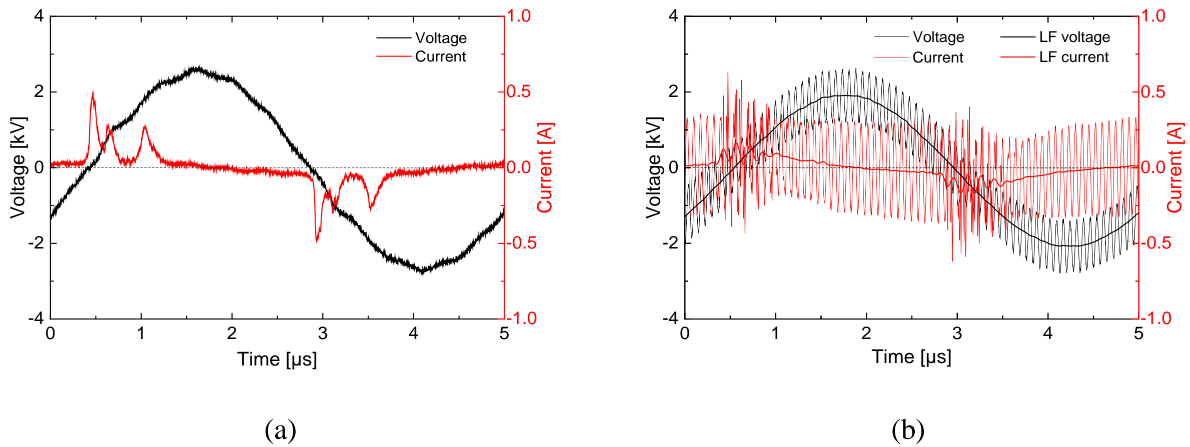

Figure. 2. Current-voltage waveforms of (a) single LF discharge (P_{LF} = 200 W, P_{RF} = 0 W) and (b) DF discharge (P_{LF} = 100 W, P_{RF} = 100 W).

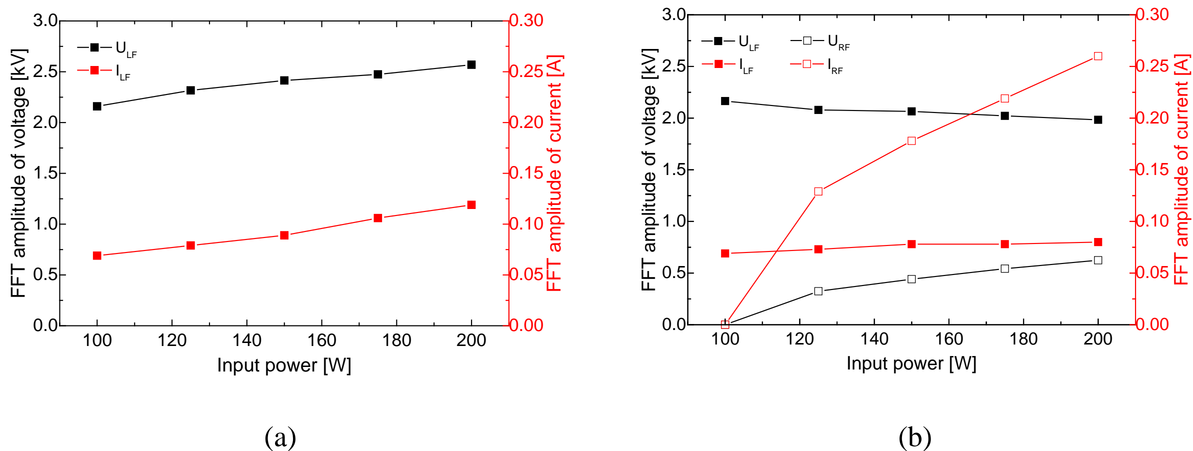

Public

Figure. 3. Fast Fourier transform (FFT) amplitudes of voltage and current with the total input power increasing from 100 W to 200 W: (a) single LF discharge and (b) DF discharge in which LF power is maintained at 100 W.

3.2 Discharge emission

For AP-PECVD process, the properties (e.g. chemistry, morphology, etc.) of deposited thin films are closely related to the regimes and the parameters of discharges [9]. The study of plasma behaviour therefore is essential to obtain a better control over the thin film growth. In this section, the side-view, normalized emission of the single LF and DF discharges with an integration time of 1.6 ms was obtained, see Figure. 4. The corresponding intensity profiles integrated in vertical and horizontal directions are shown in Figure. 5 and Figure. 6, respectively.

Form Figure. 4, the discharges under all conditions exhibit a similar "glow-like" structure with two bright luminous layers closed to the surface of dielectric barriers, while the bulk region is less bright. The discharge intensity is gradually enhanced with an increased input power, the discharge area and the uniformity however are largely affected by the power composition. For the single LF discharge, with the input power increasing from 100 W to 200 W, the discharge area gradually expands from ~12 mm to ~16 mm, as shown in Figure. 4(a)-(e) and Figure. 5(a)-(e). Under similar conditions with two curved electrodes, it was previously observed that the discharge preferentially ignites in the centre of the electrodes where the electric field is highest and then splits into two ionization waves propagating in the opposite directions [44]. After the positive streamer front arrives at the cathode region, a surface charge is quickly deposited on the dielectric surface resulting in a reduction of electric field and thus the extinction of ionization. The transverse electric field however is still high at the radical periphery of the initial current spot, thus providing a development of the transverse ionization wave [44]. In this study, with a top curved electrode and a bottom flat electrode, the discharge experiences a similar behaviour as it first ignites in the centre and then laterally propagates (results not shown here). As the input LF voltage increases, the transverse electric field and thus the lateral ionization wave propagation is enhanced, resulting in an expansion of the discharge area as a function of the input LF power. Filaments are observed under all conditions especially near the boundaries where the gas gap is larger and the plasma density is lower, see Figure. 4(a)-(e) and Figure. 5(a)-(e). In addition, due to the gas flow direction (from left to right), filaments are more obvious in the outlet area where the ambient air is mixed.

For the DF discharges, with the RF power increasing from 0 W to 100 W, the discharge area expands slightly from ~12 mm to ~13 mm, as shown in Figure. 4(f)-(j) and Figure. 5(f)-(j). In this case, the transverse electric field is mainly controlled by the LF power which is constant (100 W). The extra RF voltage mainly contributes to the oscillation of the electric field and thus the electron acceleration in the vertical direction. As a result, the discharge expansion in the lateral direction is limited. Instead, the discharge emission intensity in the bulk region is obviously enhanced compared to the single LF discharges, see Figure. 6. In addition, as previously discussed in Ref. [20], due to the periodic oscillation of the RF electric field, the discharge development is slowed down with a lower amplitude and a longer duration of the LF discharge current. The discharge uniformity therefore is significantly improved as the filament is almost invisible even in the boundary areas, see Figure. 4(f)-(j) and Figure. 5(f)-(j).

As previously introduced, to enhance the deposition rate and thus the throughput of the thin films, a higher plasma power density is required. However, increasing the discharge power can result in the formation of micro-discharges [45]. The micro-discharges are strongly non-uniform and can locally heat and damage the forming film [9], leading to the formation of macro-defects such as pinholes in the deposited thin films that limit the barrier permeation performance [12]. By applying an extra RF voltage to the LF voltage, a higher power can be input into the discharge resulting in an increased plasma density. Moreover, the discharge uniformity is improved with less filaments, making the DF excitation possibly an effective approach to further enhance the deposition rate as well as the barrier permeation performance with less defects.

Public

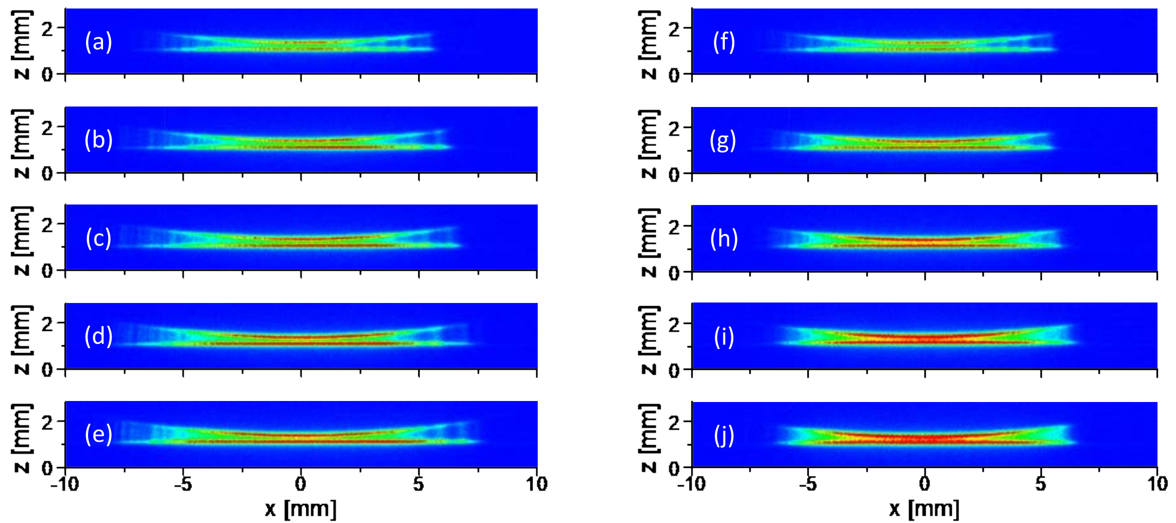

Figure. 4. Side-view integrated discharge emission with an exposure time of 1.6 ms. Left: single LF discharges with power of (a) 100 W, (b) 125 W, (c) 150 W, (d) 175 W and (e) 200 W; Right: DF discharges with LF power of 100 W and RF power of (f) 0 W, (g) 25 W, (h) 50 W, (i) 75 W and (j) 100 W. The gas is injected from left to right of the discharge area. The colour scale is normalized to condition (j).

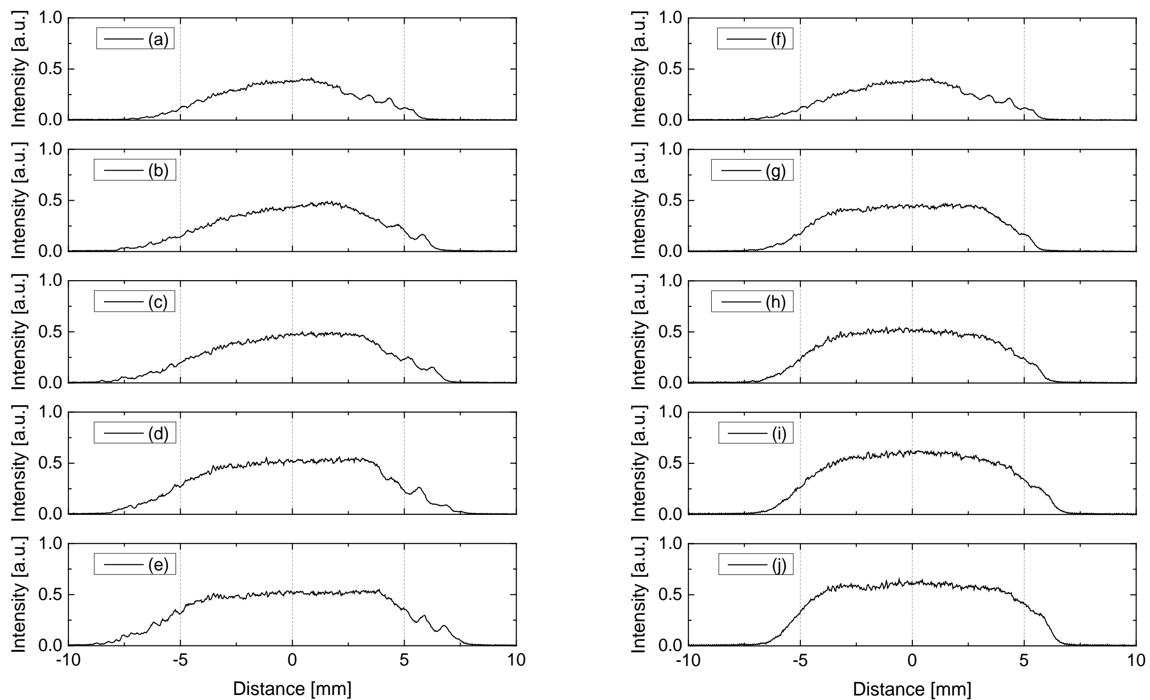

Figure. 5. Normalized intensity profiles of the discharge emission integrated in vertical direction. Left: single LF discharges with power of (a) 100 W, (b) 125 W, (c) 150 W, (d) 175 W and (e) 200 W; Right: DF discharges with LF power of 100 W and RF power of (f) 0 W, (g) 25 W, (h) 50 W, (i) 75 W and (j) 100 W. The gas is injected from left to right of the discharge area.

Public

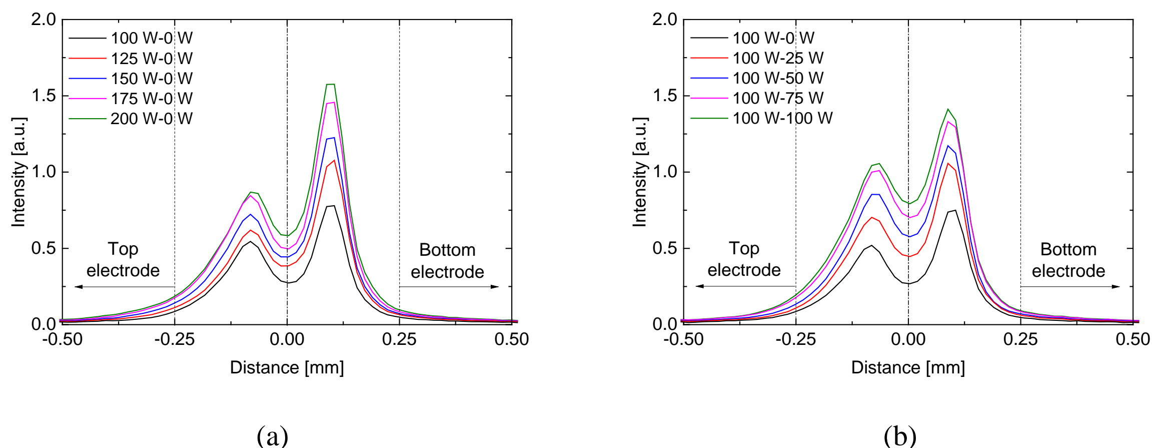

Figure. 6. Normalized intensity profiles of the discharge emission integrated in horizontal direction of (a) single LF discharges and (b) DF discharges.

3.3 Properties of the deposited thin films

Utilizing the LF and DF excitations as the plasma source, silica-like thin films with a thickness of ~ 400 nm were deposited on the polymeric susbtrates. The atomic composition and the surface morphology of the deposited thin films were determined by ATR-FTIR absorption spectroscopy and scanning electron microscopy (SEM), respectively.

Figure. 7 presents the normalized *un*-polarized ATR-FTIR absorption spectra of the silica-like barrier layers deposited by AP-PECVD with LF and DF excitations. All the spectra are normalized to the maximal signal of the main peak around 1100-1000 cm^{-1}. The main absorption band from ~1200 to ~1000 cm^{-1} can be assigned to the asymmetrical stretching of the Si-O-Si group overlapped with C-O-C and Si-O-C asymmetric stretching as well as Si-CH_2-Si [46–53]. The peak at ~1270 cm^{-1} (corresponding to Si-$(CH_3)_n$ groups with n = 1, 2, 3) is due to the symmetric bending mode of methyl groups in Si-CH_3 [46,54], indicating the existence of carbon in the deposited barriers. The carbon content can be further traced by the presence of the absorption features related to Si-C and Si-$(CH_3)_x$: the peaks at 905 cm^{-1} and 800 cm^{-1} are assigned to Si-C stretching and CH_3 rocking in Si-$(CH_3)_2$, whereas those observed at 840 cm^{-1} and 764 cm^{-1} are attributed to Si-C stretching and CH_3 rocking in Si-$(CH_3)_3$ [46,53,55–57]. It needs to be noted that the absorption band at 800 cm^{-1} also contains a contribution due to Si-O-Si bending [10,46,58]. Besides, the intense signal at 905 cm^{-1} can be partly related to silanol (Si-OH) group [58]. To further show the influence of the input power on the thin film properties, the difference of the normalized ATR-FTIR absorption spectra in Figure. 7 with a reference condition of LF discharge was calculated, as presented in Figure. 8.

From Figure. 7(a), (b) and Figure. 8(a), (b), with the total input power increasing from 100 W to 200 W, the CH_3-related peaks (~1270, ~840, ~800 and ~764 cm^{-1}) gradually decrease. The peak at 905 cm^{-1} slightly shifts towards higher wavenumbers, suggesting an enhancement of Si-OH in the films as the Si-$(CH_3)_x$ groups are removed. In addition, the main peak of the Si-O-Si group shifts from ~1035 cm^{-1} to a higher wavenumber, and the full width at half-maximum (FWHM) gradually increases. The shifting of the Si-O-Si asymmetric stretching band to the higher wavenumber indicates a larger size of chains in the cross-linked network [53] and a higher thin film density [59,60]. Some researchers also claimed that the Si–O-Si shifting is attributed to variation of bond angle [46,49], and the broadening of the band is a

Public

manifestation of a statistical distribution of different bonding arrangements at each silicon atom site [49]. However, since Si-O-C and C-O-C groups are located in this range (1200-1000 cm^{-1}) [49,51], it needs to be noted that the shifting and broadening can also be attributed to the enhancement of oxidized carbon incorporation in the layer [61]. From Figure. 7(c) and Figure. 8(c), with the same amount of total input power (200 W) but different power composition (LF and DF), the absorption peaks at ~1270, ~905, and ~764 cm^{-1} are relatively constant, the absorption peaks at ~840 and ~800 cm^{-1} are slightly changed. The main peak of Si-O-Si however exhibits a more pronounced shifting to ~1075 cm^{-1} with the DF excitation (P_{LF} = 100 W, P_{RF} = 100 W) than the LF excitation (P_{LF} = 200 W, P_{RF} = 0 W) (to ~1050 cm^{-1}).

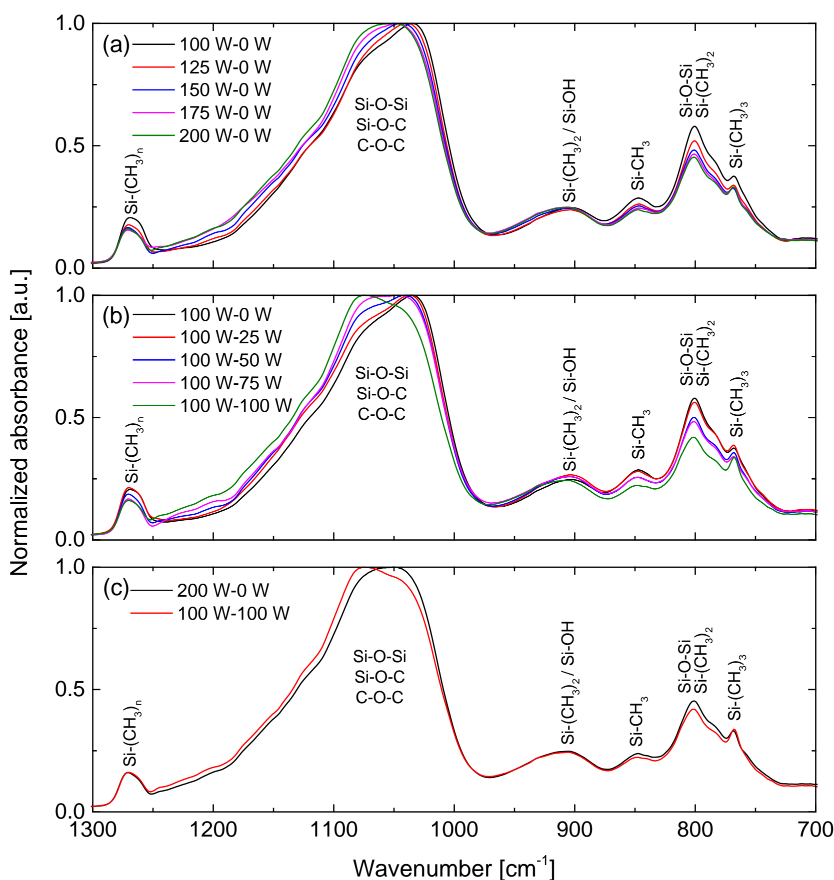

Figure. 7. Normalized *un*-polarized ATR-FTIR absorption spectra of the deposited silica-like thin films in the range of 1300-700 cm^{-1}: (a) single LF discharges, P_{LF} = 100-200 W, (b) DF discharges, P_{LF} = 100 W, P_{RF} = 0-100 W and (c) LF (P_{LF} = 200 W, P_{RF} = 0 W) vs DF (P_{LF} = 100 W, P_{RF} = 100 W).

Public

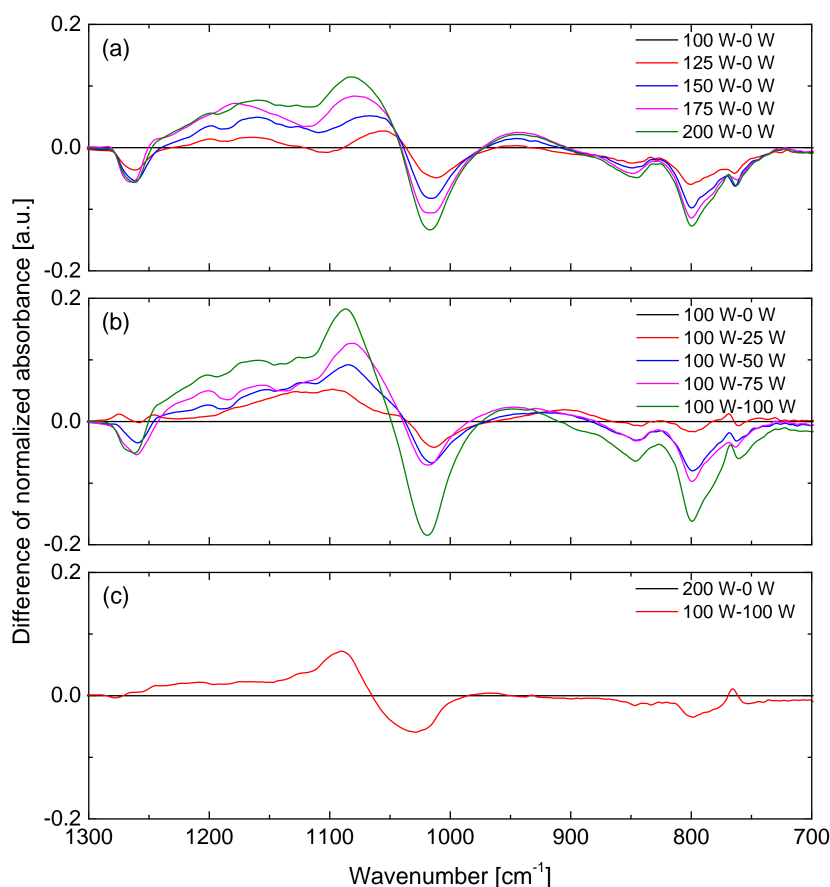

Figure. 8. Difference of the normalized ATR-FTIR absorption spectra in Figure. 7: (a) single LF discharges, P_{LF} = 100-200 W, (b) DF discharges, P_{LF} = 100 W, P_{RF} = 0-100 W and (c) LF (P_{LF} = 200 W, P_{RF} = 0 W) vs DF (P_{LF} = 100 W, P_{RF} = 100 W). The reference condition is (P_{LF} = 100 W, P_{RF} = 0 W) in (a) and (b), and (P_{LF} = 200 W, P_{RF} = 0 W) in (c).

It is known that the deposited thin film properties are closely related to the plasma parameters e.g. gas temperature, electron density and so on [9]. An increased input power leads to a higher gas temperature, resulting in a decrease in the content of carbon and hydrogen and an increase in the oxygen-to-silicon ratio in the films [62]. In addition, a higher power also leads to a higher electron density, which causes a more efficient HMDSO depletion by electron impact and (multiple) breaking of the comparably weak Si-CH_3 bonds [63]. As a result, with the input power increasing, a more efficient oxidation process of the methyl (CH_3) groups is observed as evidenced by a reduction of hydrocarbon groups and an increase of silicon and carbon oxides groups. For the DF excitation, the high frequency voltage allows to trap the electrons in the plasma bulk with less electron loss at the surface and leads to a higher power coupled into electrons [39,64]. This helps to maintain a high plasma density and enhance the elastic collision and thus the gas temperature [39,65,66]. As a result, with the same amount of input power, the DF excitation reveals a more efficient breaking of Si-CH_3 bonds and thus a more oxidized thin film.

Furthermore, the surface morphology of the deposited thin films was determind by scanning electron microscopy (SEM). The surfaces were coated with a thin conducting layer of Ti to prevent the charge building up before the SEM measurement. Figure. 9 presents the typical top-view micrographs of the samples using LF and DF excitations. It was revealed that the surface is not smooth under all experimental conditions, and the surface morphology largely depends on the input power. With relatively low input power (125 W), small dusty-like particles with a diameter of ~20 to ~50 nm appear

Public

on the surface, see Figure. 9(a) and (c). With a higher LF power (P_{LF} = 200 W, P_{RF} = 0 W), the surface exhibits a fractal texture with more closely linked features, see Figure. 9(b). With a DF power (P_{LF} = 100 W, P_{RF} = 100 W), however, the surface features are in a "sponge-like" shape, see Figure. 9(d). This phenomenon is believed to be related to the different plasma parameters e.g. gas temperature and electron density and thus the different thin film growth mechanisms due to the power composition. The DF excitation leads to a more efficient HMDSO depletion, as evidenced by the ATR-FTIR spectra and surface morphology.

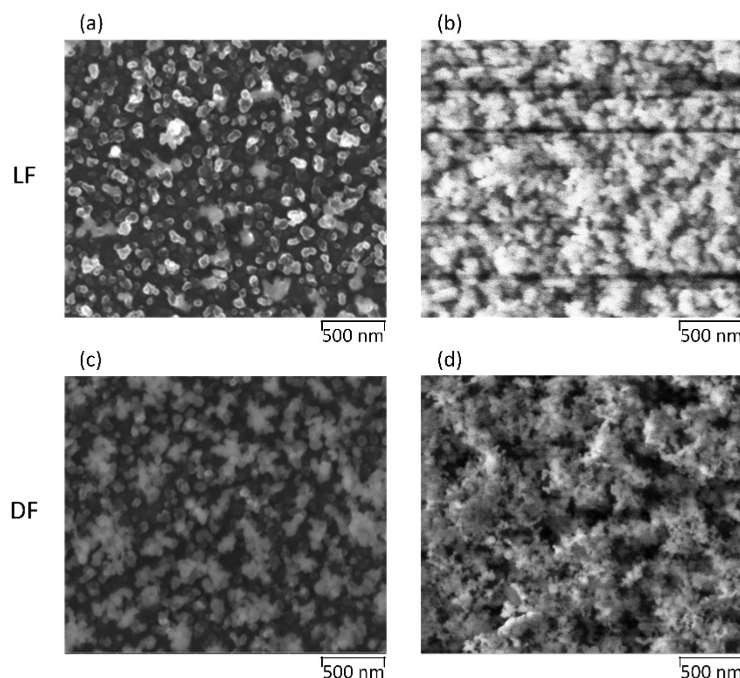

Figure. 9. Scanning electron microscopy (SEM) images illustrating the surface morphology of the deposited silica-like thin films: (a) P_{LF} = 125 W, P_{RF} = 0 W, (b) P_{LF} = 200 W, P_{RF} = 0 W, (c) P_{LF} = 100 W, P_{RF} = 25 W and (d) P_{LF} = 100 W, P_{RF} = 100 W.

4. Conclusions

In this work, a dual frequency (DF) excitation consisting of 200 kHz and 13.56 MHz frequencies was employed as the plasma source for the atmospheric pressure plasma enhanced chemical vapour deposition. With $Ar/O_2/N_2$ mixture as the working gas and HMDSO as the precursor, silica-like thin films were synthesized on the flexible polyethylene 2, 6 naphthalate substrates in a roll-to-roll reactor. The plasma behaviour including the electrical characteristics and the discharge emission was studied. The resulting silica-like thin film properties e.g. chemical microstructure and surface morphology were characterized using ATR-FTIR and SEM, respectively. It was found that the increase of LF power results in an expansion of the discharge area and the generation of filaments near the boundaries. By using a DF excitation, the expansion of the discharge area is limited, instead the plasma density increases more in the bulk region. Furthermore, the DF excitation presents a capability of improving plasma uniformity with less filaments, which could help to reduce the macro-defects and improve the permeation performance of the deposited barrier layers. According to the ATR-FTIR analysis, increasing input power leads to an improved microstructure of the silica barrier layers with less hydrocarbon units and more oxidized film structures. This is further evidenced by the SEM surface morphology showing sponge-like network structures. Due to the increased electron density and gas temperature, the DF excitation demonstrates a more efficient breaking of $Si-CH_3$ bonds.

Acknowledgement

This work was supported by the Industrial Partnership Programme i31 (APFF) that is carried out under an agreement between FUJIFILM Manufacturing Europe BV and FOM, which is part of the Netherlands

Public

Organization for Scientific Research (NWO). The author would like to thank Wim Melissen (Dutch Institute for Fundamental Energy Research, Eindhoven, The Netherlands), Bruno Korngold, Rinie van Beijnen and Emile Gommers (FUJIFILM Manufacturing Europe B.V., Tilburg, The Netherlands) for their technical assistance.

References

[1] Lewis J 2006 Material challenge for flexible organic devices *Mater. Today* **9** 38–45

[2] Weaver M S, Michalski L A, Rajan K, Rothman M A, Silvernail J A, Brown J J, Burrows P E, Graff G L, Gross M E, Martin P M, Hall M, Mast E, Bonham C, Bennett W and Zumhoff M 2002 Organic light-emitting devices with extended operating lifetimes on plastic substrates *Appl. Phys. Lett.* **81** 2929–31

[3] Chwang A B, Rothman M A, Mao S Y, Hewitt R H, Weaver M S, Silvernail J A, Rajan K, Hack M, Brown J J, Chu X, Moro L, Krajewski T and Rutherford N 2003 Thin film encapsulated flexible organic electroluminescent displays *Appl. Phys. Lett.* **83** 413–5

[4] Seo S W, Jung E, Lim C, Chae H and Cho S M 2012 Water permeation through organic-inorganic multilayer thin films *Thin Solid Films* **520** 6690–4

[5] Han Y C, Kim E, Kim W, Im H G, Bae B S and Choi K C 2013 A flexible moisture barrier comprised of a SiO2-embedded organic-inorganic hybrid nanocomposite and Al2O3for thin-film encapsulation of OLEDs *Org. Electron. physics, Mater. Appl.* **14** 1435–40

[6] Morlier A, Cros S, Garandet J P and Alberola N 2013 Gas barrier properties of solution processed composite multilayer structures for organic solar cells encapsulation *Sol. Energy Mater. Sol. Cells* **115** 93–9

[7] Wong W S and Salleo A 2009 *Flexible Electronics: Materials and Applications* ed W S Wong and A Salleo (New York: Springer Science+Business Media)

[8] Bahroun K, Behm H, Mitschker F, Awakowicz P, Dahlmann R and Hopmann C 2014 Influence of layer type and order on barrier properties of multilayer PECVD barrier coatings *J. Phys. D. Appl. Phys.* **47**

[9] Massines F, Sarra-Bournet C, Fanelli F, Naudé N and Gherardi N 2012 Atmospheric pressure low temperature direct plasma technology: Status and challenges for thin film deposition *Plasma Process. Polym.* **9** 1041–73

[10] Starostin S A, Premkumar P A, Creatore M, De Vries H, Paffen R M J and Van De Sanden M C M 2010 High current diffuse dielectric barrier discharge in atmospheric pressure air for the deposition of thin silica-like films *Appl. Phys. Lett.* **96** 061502

[11] Starostin S A, Creatore M, Bouwstra J B, Van De Sanden M C M and De Vries H W 2015 Towards roll-to-roll deposition of high quality moisture barrier films on polymers by atmospheric pressure plasma assisted process *Plasma Process. Polym.* **12** 545–54

[12] Elam F M 2017 *Atmospheric pressure-plasma enhanced chemical vapour deposition of silica: Characterization and control of porosity in multi-layer encapsulation films* (Eindhoven University of Technology)

[13] Vallee C, A G, Granier A, van der Lee A, J D and Marliere C 2000 Inorganic to organic crossover in thin films deposited from O2/TEOS plasmas *J. Non. Cryst. Solids* **272** 163–73

[14] Paul E. Burrows; Gordon L. Graff; Mark E. Gross; Peter M. Martin; Michael Hall; Eric Mast; Charles C. Bonham; Wendy D. Bennett; Lech A. Michalski; Michael S. Weaver; Julie J. Brown; D. Fogarty; Linda S. Sapochak 2001 Gas permeation and lifetime tests on polymer-based barrier coatings *Proc. SPIE* p 4105

[15] nagai shingo 2015 A numerical study for the integrative definition of moisture-barrier performance regarding multilayered barrier-stack for an encapsulated system *Surf. Coatings Technol.* **267** 59–64

[16] Aresta G, Premkumar P A, Starostin S A, De Vries H, Van De Sanden M C M and Creatore M 2010 Optical characterization of plasma-deposited SiO2-like layers on anisotropic polymeric substrates *Plasma Process. Polym.* **7** 766–74

[17] Elam F M, Starostin S A, Meshkova A S, van der Velden-Schuermans B C A M, Bouwstra J B, van de Sanden M C M and de Vries H W 2016 Atmospheric pressure roll-to-roll plasma enhanced CVD of high quality silica-like bilayer encapsulation films *Plasma Process. Polym.* **14** 1600143

[18] Gherardi N, Gouda G, Gat E, Ricard A and Massines F 2000 Transition from glow silent discharge to micro-discharges in nitrogen gas *Plasma Sources Sci. Technol.* **9** 340–6

Public

[19] Liu Y, Starostin S A, Peeters F J J, Van De Sanden M C M and De Vries H W 2018 Atmospheric-pressure diffuse dielectric barrier discharges in Ar/O2gas mixture using 200 kHz/13.56 MHz dual frequency excitation *J. Phys. D. Appl. Phys.* **51**

[20] Liu Y, Peeters F J J, Starostin S A, Van De Sanden M C M and De Vries H W 2018 Improving uniformity of atmospheric-pressure dielectric barrier discharges using dual frequency excitation *Plasma Sources Sci. Technol.* **27**

[21] Liu Y, van't Veer K, Peeters F J J, Mihailova D B, van Dijk J, Starostin S A, van de Sanden M C M and de Vries H W 2018 Numerical simulation of atmospheric-pressure 200 kHz/13.56 MHz dual-frequency dielectric barrier discharges *Plasma Sources Sci. Technol.* **27** 105016

[22] Kim D-H, Kim Y-D, Cho S-W, Kim Y-S and Chung C-W 2014 Investigation of plasma diagnostics using a dual frequency harmonic technique *J. Appl. Phys.* **116** 093302

[23] Denda T, Miyoshi Y, Komukai Y, Goto T, Petrović Z L and Makabe T 2004 Functional separation in two frequency operation of an inductively coupled plasma *J. Appl. Phys.* **95** 870–6

[24] Kitajima T, Takeo Y, Petrović Z L and Makabe T 2000 Functional separation of biasing and sustaining voltages in two-frequency capacitively coupled plasma *Appl. Phys. Lett.* **77** 489–91

[25] Bruneau B, Gans T, O'Connell D, Greb A, Johnson E V. and Booth J P 2015 Strong ionization asymmetry in a geometrically symmetric radio frequency capacitively coupled plasma induced by sawtooth voltage waveforms *Phys. Rev. Lett.* **114** 125002

[26] Sharma S and Turner M M 2013 Simulation study of stochastic heating in single-frequency capacitively coupled discharges with critical evaluation of analytical models *Plasma Sources Sci. Technol.* **22** 035014

[27] Kawamura E, Lieberman M A and Lichtenberg A J 2006 Stochastic heating in single and dual frequency capacitive discharges *Phys. Plasmas* **13**

[28] Gans T, Schulze J, O'Connell D, Czarnetzki U, Faulkner R, Ellingboe A R and Turner M M 2006 Frequency coupling in dual frequency capacitively coupled radio-frequency plasmas *Appl. Phys. Lett.* **89** 261502

[29] Waskoenig J and Gans T 2010 Nonlinear frequency coupling in dual radio-frequency driven atmospheric pressure plasmas *Appl. Phys. Lett.* **96** 181501

[30] Ziegler D, Trieschmann J, Mussenbrock T, Brinkmann R P, Schulze J, Czarnetzki U, Semmler E, Awakowicz P, O'Connell D and Gans T 2010 The influence of the relative phase between the driving voltages on electron heating in asymmetric dual frequency capacitive discharges *Plasma Sources Sci. Technol.* **19** 045001

[31] Boyle P C, Robiche J and Turner M M 2004 Modelling of the dual frequency capacitive sheath in the intermediate pressure range *J. Phys. D. Appl. Phys.* **37** 1451–8

[32] Boyle P C, Ellingboe A R and Turner M M 2004 Independent control of ion current and ion impact energy onto electrodes in dual frequency plasma devices *J. Phys. D. Appl. Phys.* **37** 697–701

[33] Sahu B B, Yin Y Y, Tsutsumi T, Hori M and Han J G 2016 The role of plasma chemistry on functional silicon nitride film properties deposited at low-temperature by mixing two frequency powers using PECVD *Phys. Chem. Chem. Phys.* **18** 13033–44

[34] Sahu B B, Yin Y, Lee J S, Han J G and Shiratani M 2016 Plasma diagnostic approach for the low-temperature deposition of silicon quantum dots using dual frequency PECVD *J. Phys. D. Appl. Phys.* **49** 395203

[35] Shin K S, Sahu B B, Han J G and Hori M 2015 Utility of dual frequency hybrid source for plasma and radical generation in plasma enhanced chemical vapor deposition process *Jpn. J. Appl. Phys.* **54**

[36] Piallat F, Vallée C, Gassilloud R, Michallon P, Pelissier B and Caubet P 2014 PECVD RF versus dual frequency: an investigation of plasma influence on metal–organic precursors' decomposition and material characteristics *J. Phys. D. Appl. Phys.* **47** 185201

[37] Bieder A, Gruniger A and Rudolf von Rohr P 2005 Deposition of SiOx diffusion barriers on flexible packaging materials by PECVD *Surf. Coatings Technol.* **20** 928–31

[38] Jin S B, Lee J S, Choi Y S, Choi I S and Han J G 2011 High-rate deposition and mechanical properties of SiOx film at low temperature by plasma enhanced chemical vapor deposition with the dual frequencies ultra high frequency and high frequency *Thin Solid Films* **519** 6334–8

[39] Liu D, Yang A, Wang X, Chen C, Rong M and Kong M G 2016 Electron heating and particle fluxes in

Public

dual frequency atmospheric-pressure helium capacitive discharge *J. Phys. D. Appl. Phys.* **49** 49LT01

[40] Oneill C, Waskoenig J and Gans T 2012 Tailoring electron energy distribution functions through energy confinement in dual radio-frequency driven atmospheric pressure plasmas *Appl. Phys. Lett.* **101** 1–5

[41] Starostine S, Aldea E, de Vries H, Creatore M and van de Sanden M C M 2007 Atmospheric pressure barrier discharge deposition of silica-like films on polymeric substrates *Plasma Process. Polym.* **4** 440–4

[42] Premkumar P A, Starostin S A, de Vries H, Paffen R M J, Creatore M, Eijkemans T J, Koenraad P M and de Sanden M C M van 2009 High Quality SiO_2 -like Layers by Large Area Atmospheric Pressure Plasma Enhanced CVD: Deposition Process Studies by Surface Analysis *Plasma Process. Polym.* **6** 693–702

[43] Akishev Y S, Dem'yanov A V., Karal'nik V B, Pan'kin M V. and Trushkin N I 2001 Pulsed Regime of the Diffusive Mode of a Barrier Discharge in Helium *Plasma Phys. Reports* **27** 164–71

[44] Starostin S A, Welzel S, Liu Y, Velden-Schuermans B van der, Bouwstra J B, van de Sanden M C M and de Vries H W 2015 Dynamics of the atmospheric pressure diffuse dielectric barrier discharge between cylindrical electrodes in roll-to-roll PECVD reactor *Eur. Phys. J. Appl. Phys.* **71** 20803

[45] Bazinette R, Subileau R, Paillol J and Massines F 2014 Identification of the different diffuse dielectric barrier discharges obtained between 50 kHz to 9 MHz in Ar/NH3 at atmospheric pressure *Plasma Sources Sci. Technol.* **23** 035008

[46] Ziari Z, Nouicer I, Sahli S, Rebiai S, Bellel A, Segui Y and Raynaud P 2013 Chemical and electrical properties of HMDSO plasma coated polyimide *Vacuum* **93** 31–6

[47] Kashiwagi K, Yoshida Y and Murayama Y 1991 Hybrid films formed from hexamethyldisiloxane and sio by plasma process *Jpn. J. Appl. Phys.* **30** 1803–7

[48] Kim M T 1997 Deposition behavior of hexamethydisiloxane films based on the FTIR analysis of Si-O-Si and Si-CH3bonds *Thin Solid Films* **311** 157–63

[49] Grill A and Neumayer D A 2003 Structure of low dielectric constant to extreme low dielectric constant SiCOH films: Fourier transform infrared spectroscopy characterization *J. Appl. Phys.* **94** 6697–707

[50] Deshmukh S C and Aydil E S 1995 Investigation of SiO_2 plasma enhanced chemical vapor deposition through tetraethoxysilane using attenuated total reflection Fourier transform infrared spectroscopy *J. Vac. Sci. Technol. A Vacuum, Surfaces, Film.* **13** 2355–67

[51] Mota R P, Galv??o D, Durrant S F, De Moraes M A B, de Oliveira Dantas S and Cant??o M 1995 HMDSO plasma polymerization and thin film optical properties *Thin Solid Films* **270** 109–13

[52] Creatore M, Palumbo F and Agostino R 2002 Deposition of SiO x Films from Hexamethyldisiloxane / Oxygen Radiofrequency Glow Discharges : Process Optimization by Plasma Diagnostics *Plasma Polym.* **7** 291–310

[53] Supiot P, Vivien C, Granier A, Bousquet A, Mackova A, Escaich D, Clergereaux R, Raynaud P, Stryhal Z and Pavlik J 2006 Growth and modification of organosilicon films in PECVD and remote afterglow reactors *Plasma Process. Polym.* **3** 100–9

[54] Lamendola R, D'Agostino R and Fracassi F 1997 Thin film deposition from hexamethyldisiloxane fed glow discharges *Plasmas Polym.* **2** 147–64

[55] Rau C and Kulisch W 1994 Mechanisms of plasma polymerization of various silico-organic monomers *Thin Solid Films* **249** 28–37

[56] Zanini S, Riccardi C, Orlandi M, Esena P, Tontini M, Milani M and Cassio V 2005 Surface properties of HMDSO plasma treated polyethylene terephthalate *Surf. Coatings Technol.* **200** 953–7

[57] Ji Y Y, Chang H K, Hong Y C and Lee S H 2009 Water-repellent improvement of polyester fiber via radio frequency plasma treatment with argon/hexamethyldisiloxane (HMDSO) at atmospheric pressure *Curr. Appl. Phys.* **9** 253–6

[58] Fanelli F, Lovascio S, D'Agostino R, Arefi-Khonsari F and Fracassi F 2010 Ar/HMDSO/O2 fed atmospheric pressure DBDs: Thin film deposition and GC-MS investigation of by-products *Plasma Process. Polym.* **7** 535–43

[59] Zanini S, Riccardi C, Orlandi M and Grimoldi E 2008 Characterisation of SiOxCyHzthin films deposited by low-temperature PECVD *Vacuum* **82** 290–3

[60] Li K, Gabriel O and Meichsner J 2004 Fourier transform infrared spectroscopy study of molecular structure formation in thin films during hexamethyldisiloxane decomposition in low pressure rf discharge

Public

[61] Premkumar P A, Starostin S A, De Vries H, Creatore M, Koenraad P M and Van De Sanden M C M 2013 Morphological description of ultra-smooth organo-silicone layers synthesized using atmospheric pressure dielectric barrier discharge assisted PECVD *Plasma Process. Polym.* **10** 313–9

[62] Trunec D, Zajíčková L, Buršíková V, Studnička F, Sťahel P, Prysiazhnyi V, Peřina V, Houdková J, Navrátil Z and Franta D 2010 Deposition of hard thin films from HMDSO in atmospheric pressure dielectric barrier discharge *J. Phys. D. Appl. Phys.* **43** 225403

[63] Wallimann R, Roth C and Rudolf von Rohr P 2018 Nanoparticle production from HMDSO in atmospheric pressure argon-oxygen plasma *Plasma Process. Polym.* **15** e1700202

[64] Liu D W, Shi J J and Kong M G 2007 Electron trapping in radio-frequency atmospheric-pressure glow discharges *Appl. Phys. Lett.* **90** 2005–8

[65] Zhou Y J, Yuan Q H, Li F, Wang X M, Yin G Q and Dong C Z 2013 Nonequilibrium atmospheric pressure plasma jet using a combination of 50 kHz/2 MHz dual-frequency power sources *Phys. Plasmas* **20** 113502

[66] Yang A, Rong M, Wang X, Liu D and Kong M G 2013 Variable radio-frequency cold atmospheric He+O2 discharges: from electron-heating mechanism to reactive species delivery *J. Phys. D. Appl. Phys.* **46** 415201

Public